



Cite this: DOI: 10.1039/c8nr04376k

## Tunable WSe<sub>2</sub>–CdS mixed-dimensional van der Waals heterojunction with a piezo-phototronic effect for an enhanced flexible photodetector†

Pei Lin,<sup>a,b</sup> Laipan Zhu,<sup>a,b</sup> Ding Li,<sup>a,b</sup> Liang Xu<sup>a,b</sup> and Zhong Lin Wang  <sup>\*a,b,c</sup>

Due to the absence of bond fracture and atomic reconstruction under strain, vdWs structures hold great promise in flexible electronic/optoelectronic applications. Besides all-2D heterojunctions, the dangling-bond-free surfaces of 2D materials also enable vdWs interaction with other materials of different dimensionalities, forming mixed-dimensional vdWs heterostructures. Such structures allow a much broader selection of materials and may provide a promising approach to compensate for the intrinsic weakness of 2D crystals before realizing their full potential. In this study, we present the fabrication of a WSe<sub>2</sub>–CdS mixed-dimensional vdWs p–n heterojunction for flexible photodetection. A strain-tunable vdWs interface was demonstrated and the photoresponse was dramatically enhanced with the piezo-phototronic effect. The photocurrent can be increased by ~110% under a compressive strain of –0.73% and the corresponding photoresponsivity reaches up to 33.4 A W<sup>–1</sup>. The enhancement originates from realigned local energy-band tilting at the WSe<sub>2</sub>–CdS interface by strain-induced piezopolarization, which promotes the transport process of photoexcited carriers. Our work provides a new route to a tunable vdWs interface other than with electrostatic gating, which may inspire the development of novel flexible vdWs optoelectronics.

Received 30th May 2018,  
Accepted 11th July 2018

DOI: 10.1039/c8nr04376k

rsc.li/nanoscale

### Introduction

With the emergence of transition-metal dichalcogenides and other materials such as SnS<sub>2</sub>, SnSe<sub>2</sub> and black phosphorus as novel two-dimensional (2D) atomic crystals, artificial 2D–2D van der Waals (vdWs) heterostructures with varying functionalities have been successfully assembled through a combination of disparate 2D materials without the constraint of lattice mismatch.<sup>1–7</sup> The electronic structure of such a heterojunction offers intriguing possibilities to achieve a delicate manipulation of carriers' behavior at the atomic interface and design unique devices with a specific functionality. In particular, the absence of bond fracture and atomic reconstruction under strain, in combination with the superior mechanical property of 2D materials make vdWs structures an ideal candidate for

flexible and ultrathin electronics/optoelectronics.<sup>8</sup> However, until now, large-scale production of the entire family of 2D materials with controlled quality and electronic property (defects, doping type, carrier concentration, *etc.*) still remained a significant challenge, which greatly limits the development progress of all-2D vdWs heterostructures. In a broad sense, any two passivated, dangling-bond-free surfaces bond together by means of the vdWs force; therefore mixed-dimensional vdWs heterostructures could be expected through hybridizing 2D layered atomic crystals with other materials of different dimensionalities.<sup>9</sup> Compared with the all-2D structure, such a mixed-dimensional combination reveals a much broader selection of materials and has opened up a new paradigm for functional nanomaterials integration. Moreover, it helps to harness the synergistic advantages of different dimensional materials to realize high performance electronics/optoelectronics. With the advances in synthesis, transfer and assembly techniques, multiple types of mixed-dimensional vdWs heterostructures have been demonstrated through the integration of 2D materials with 0D quantum dots, 1D carbon nanotubes and 3D crystal-line bulk Si, GaAs and other III–V semiconductors.<sup>10–16</sup>

Precise tunability over the interface property is critical to the operation of functional vdWs devices. Normally, most of the reported manipulations of the 2D p–n or Schottky junction were achieved by electrostatic gating on hard substrates

<sup>a</sup>CAS Center for Excellence in Nanoscience, Beijing Key Laboratory of Micro-nano Energy and Sensor, Beijing Institute of Nanoenergy and Nanosystems, Chinese Academy of Sciences, Beijing 100083, P. R. China

<sup>b</sup>School of Nanoscience and Technology, University of Chinese Academy of Sciences, Beijing 100049, P. R. China

<sup>c</sup>School of Material Science and Engineering, Georgia Institute of Technology, Atlanta, Georgia 30332, USA. E-mail: zhong.wang@mse.gatech.edu

†Electronic supplementary information (ESI) available. See DOI: 10.1039/c8nr04376k

(e.g., SiO<sub>2</sub>/Si).<sup>17,18</sup> However, this gate-tunable approach may not be the best choice for flexible optoelectronics as it adds extra complexity during the device fabrication and integration process, such as the deposition of dielectrics and gate electrode.<sup>19</sup> As is known, mechanical strain is ubiquitous throughout the whole process from the preparation of 2D materials, device assembly to their final operation conditions. Therefore the direct implementation of two-terminal vdWs junction modulation with external mechanical agitation would be more attractive for flexible electronics, which may give rise to great simplification of the device structure and offer a novel functionality. The piezoelectric effect, which represents the active interaction between mechanical and electrical states, could act as an enabler of such a requirement.<sup>20</sup> Although the 2D–1D mixed-dimensional vdWs heterostructure has been demonstrated, the fabrication of the corresponding flexible optoelectronics and the realization of vdWs junction modulation through mechanical strain have rarely been reported.

In this study, we present the fabrication of a 2D WSe<sub>2</sub>–1D CdS nanowire mixed-dimensional vdWs p–n heterojunction for flexible photodetection. Single-crystal CdS nanowire was selected because of its excellent mechanical property and decent piezoelectric constant. A strain-tunable vdWs heterojunction was demonstrated and the corresponding photoresponse was dramatically enhanced with the piezo-phototronic effect. Under 680 nm light illumination, the photocurrent can be increased by ~110% when applying a compressive strain of –0.73% and the photoresponsivity reaches up to 33.4 A W<sup>–1</sup>. This enhancement originates from realigned local energy-band tilting at the WSe<sub>2</sub>–CdS interface by strain-induced piezopolarization charges, which promotes the photo-excited carriers' separation and transport process. The

approach in this work offers a new route to tunable vdWs heterostructures other than with electrostatic gating, which may provide a new direction for novel vdWs structure design and enable the implementation of high-performance optoelectronics.

## Results and discussion

The *n*-CdS nanowires (NWs) used in the experiment were synthesized on silicon *via* a physical vapor deposition approach (details in Experimental section and Fig. S1†); p-type multi-layer WSe<sub>2</sub> flakes were prepared through mechanical exfoliation.<sup>21</sup> Fig. 1a shows the overall optical microscopy (OM) image of fabricated WSe<sub>2</sub>–CdS mixed-dimensional vdWs heterostructure devices. Here, polyethylene terephthalate (PET) was selected as a flexible substrate because of its good solvent-resistant property and relatively high Young's modulus, which ensures that the substrate bending-induced strain can be effectively transferred to the CdS NW.<sup>22</sup> The detailed fabrication process of the heterojunction diode is presented in Fig. 1b–d. The precise transfer of WSe<sub>2</sub> was achieved by poly(propylene carbonate) (PPC) viscoelastic stamping with the help of an accurate transfer platform equipped with micromanipulators (fabrication details in Experimental section).<sup>23,24</sup> This all-dry transfer approach avoids the use of a strong acid or alkali solution, which helps to maintain the pristine electrical/optical properties of the materials without significant degradation. According to the height profile obtained from atomic force microscopy (AFM) characterization in Fig. 1e, the thickness of the WSe<sub>2</sub> flakes was estimated to be 7 nm. The Raman and photoluminescence (PL) spectra of WSe<sub>2</sub> are shown in Fig. S2

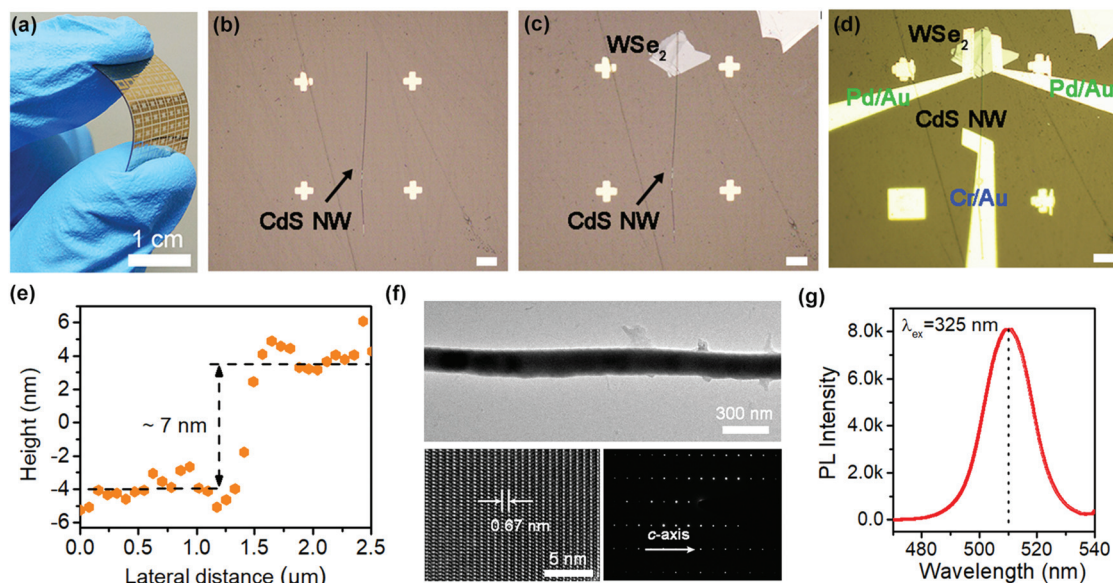


**Fig. 1** (a) OM image of a flexible 2D WSe<sub>2</sub> nanosheet–1D CdS nanowire heterojunction device. (b–d) Fabrication steps of the heterostructure device; scale bar is 20 μm. (e) The AFM height profile of the WSe<sub>2</sub> flake. (f) Low- and high-magnification TEM images of CdS and selected area electron diffraction pattern. (g) Room-temperature PL spectrum of the synthetic CdS NW.

in the ESI;† three characteristic peaks of in-plane  $E_{2g}^1$  and out-of-plane  $A_{1g}$  and  $B_{2g}$  vibration modes were observed.<sup>25</sup> Fig. 1f shows the typical transmission electron microscopy (TEM) characterization result of a single CdS NW, which reveals a good wurtzite crystalline quality and the growth direction is along [0001]. As is known, CdS possesses the most significant piezoelectric effect and the largest piezoelectric coefficient along the  $c$ -axis, which is beneficial for the following piezo-phototronic modulation of device performance.<sup>26</sup> The room-temperature CdS PL spectrum recorded with 325 nm excitation is shown in Fig. 1g. The single peak centered at 510 nm with the narrow full-width half maximum demonstrates that the synthetic CdS NW has a high-quality optical property.

The electrical measurement of the fabricated flexible device in the dark is shown in Fig. 2a, which presents a good current rectification behavior with an ideality factor of 2.69. Fig. 2b shows the photoresponse in this heterojunction diode under strain-free conditions. The measured overall  $I_{ds}$  increases significantly from 0.32 nA in the dark to 3.84 nA with 11.74 mW

$cm^{-2}$  680 nm laser illumination when a drain voltage of +2 V was applied. The photocurrent ( $I_{photo} = I_{ds} - I_{dark}$ ) shows an approximate linear dependency with optical intensity and no saturation was observed in the measured range, as plotted in Fig. 2c. The photoresponsivity, which is defined as  $I_{photo}/P_{laser}$ , where  $P_{laser}$  is the illumination power on the devices, is another critical parameter of the photodetector. Fig. 2d shows that the device reaches a responsivity of 16.2  $A W^{-1}$  at a low illumination power intensity of 16.9  $\mu W cm^{-2}$ , while the photoresponsivity decreases at higher illumination power due to the emergence of trap states in the materials or at the interface.<sup>27</sup> The  $I-t$  characteristics and stability of the flexible photodetector under various illuminations were investigated at the applied +2 V drain bias, as presented in Fig. 2e. An obvious switching behavior is observed and the ON/OFF property could be well retained within the multiple cycle tests; the inset shows the corresponding response time less than 1 s. The schematic of a home-made setup for characterizing the strain-modulated photoresponse process is shown in Fig. 2f. The strain was introduced through a two-point bending apparatus,

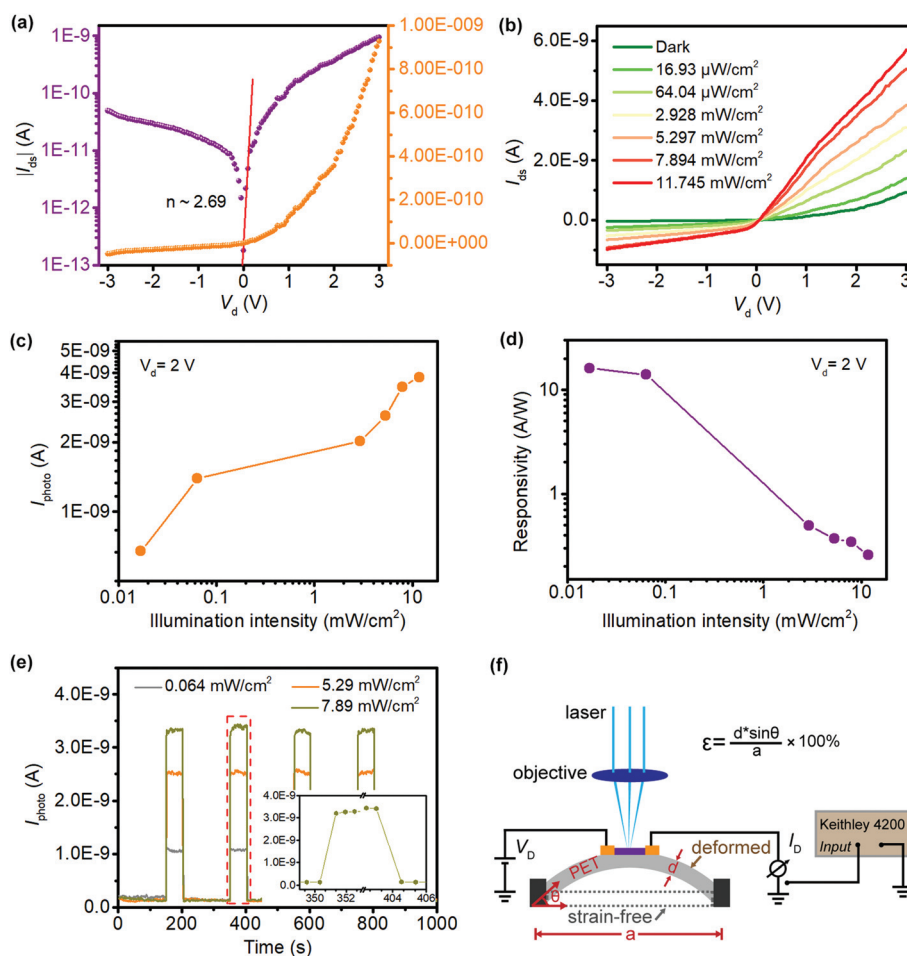


**Fig. 2** (a) Current–voltage curves of the WSe<sub>2</sub>–CdS heterostructure in the linear and logarithmic scale. (b) Photoresponse property of the device when illuminated with different 680 nm intensities. Photocurrent  $I_{photo}$  (c) and photoresponsivity (d) as a function of optical power under +2 V drain bias. (e)  $I-t$  characteristic and reproducibility of the device; the inset shows the corresponding response time. (f) Schematic of the experimental setup for calculating the applied strain and characterizing the piezo-phototronic process in the fabricated device.

and the bent PET substrate was considered as a circular arc when computing the applied strain. Besides, since the materials' dimension is substantially smaller than that of PET, the bending of the flexible substrate results in pure uniaxial tensile or compressive strain in the CdS NW and the value could be given by the equation in the inset of Fig. 2f.<sup>28</sup> Here, the negative sign is for the compressive strain and the positive sign is for the tensile strain. To avoid sample slippage and plastic deformation of the PET substrate, the applied strain was limited to 1% in the following experiment. Moreover, it is noteworthy that some of the fabricated WSe<sub>2</sub>-CdS heterojunction diodes also display an obvious photovoltaic behavior, as shown in Fig. S3.† The detailed analysis of the short-circuit current  $J_{sc}$  and open-circuit voltage  $V_{oc}$  as a function of optical power is plotted in Fig. S3b.† Under the illumination of a 13.5 mW cm<sup>-2</sup> 680 nm laser,  $V_{oc}$  of 0.29 V and  $J_{sc}$  of 138.5 pA were observed and the fill factor was about 0.28. It is believed that these performance parameters could be further improved by reducing the series resistance and device geometry optimization. As a consequence, this mixed-dimensional heterojunc-

tion also has the potential to function as a solar cell or a self-powered photodiode; a fast and reproducible switching behavior under zero bias was demonstrated and is shown in Fig. S3c in the ESI.†

To characterize the strain-modulated photodetection change, electrical transport of the diode under various applied strains without optical illumination was firstly investigated, as shown in Fig. 3a. The results indicate a strong strain dependency of the dark current. At +2 V drain bias, the output current  $I_{ds}$  increases from 0.32 nA to 1.75 nA under -0.73% compressive strain and decreases to 0.14 nA when applying 0.67% tensile strain. Besides, an obvious strain-gated vdWs junction property was demonstrated. The calculated strain-induced junction barrier height change is plotted in Fig. S4† and the turn-on voltage of the diode was effectively tuned. Such interfacial modulation may rule out the dominant contribution of the piezoresistive effect to the measured transport change, which means a change in the bulk resistivity of the materials under the applied strain.<sup>29</sup> Therefore, it can be speculated that the piezotronic effect, where strain-induced

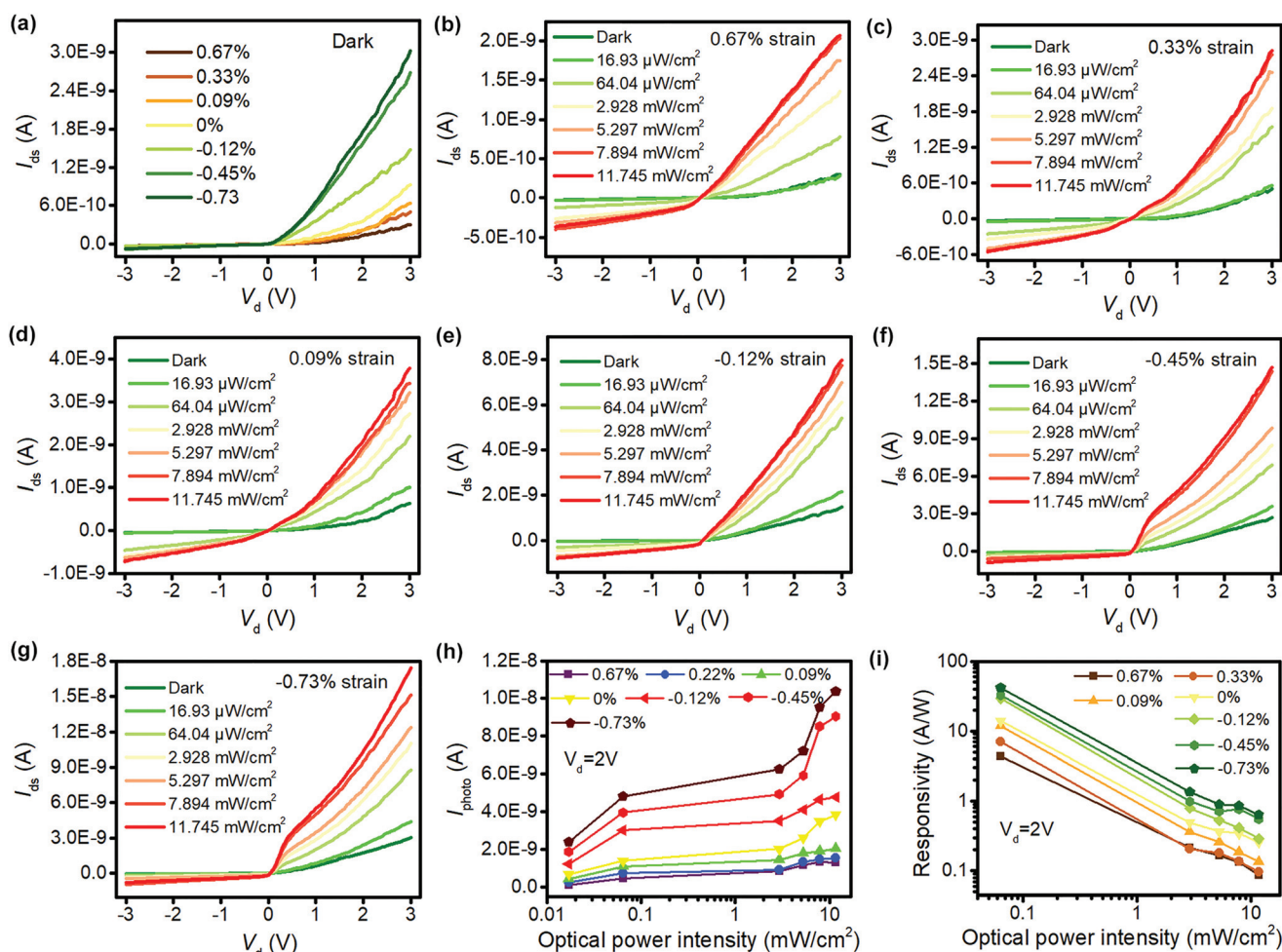


**Fig. 3** (a) Electrical transport of the fabricated device in the dark under different strains. (b–g) Photodetection performance in the flexible device under various strains when illuminated with a 680 nm laser. Strain dependence of photocurrent (h) and photoresponsivity (i) in the device under +2 V drain bias, which indicates an effective modulation of the performance with mechanical strain.

piezopolarization charges function as a “gate” signal to tune the barrier characteristic and transport behavior at the vicinity of the interface, may give rise to the observed current change.<sup>30–34</sup> Then, by illuminating with a 680 nm laser with different optical intensities, the photodetection behavior of the device was characterized under various mechanical strains, as shown in Fig. 3b–g. The corresponding photocurrent  $I_{\text{photo}}$  at +2 V drain bias was calculated and is summarized in Fig. 3h. The result shows that for each illumination intensity, the photocurrent increases with increasing compressive strain, indicating that the photoresponse performance of the vdWs heterostructure is significantly improved. At the illumination intensity of  $16.9 \mu\text{W cm}^{-2}$ , the photocurrent was enhanced from 0.32 nA to 0.65 nA when applying a  $-0.73\%$  compressive strain and the optimized photoresponsivity reaches up to  $33.4 \text{ A W}^{-1}$ , as shown in Fig. 3i. In addition, both theoretical analysis and experiments show that the spectral absorption of WSe<sub>2</sub> around 680 nm varies little under external strain, which is incompatible with the measured photocurrent change.<sup>35</sup> As the distance between the devices and the illumination source will change when bending the flexible substrate, the resulted variation in illumination power intensity should also be taken into account when determining the main reason for the change in the detection properties. The results in Fig. S5† indicate that the  $I_{\text{photo}}$  change due to distance variations is much weaker than the measured data in Fig. 3, which are further evidence that the piezo-phototronic effect should dominate the whole performance modulation process. The temporal response and repeatability of the diode under different strains and  $7.89 \text{ mW cm}^{-2}$  illumination at +2 V drain bias are presented in Fig. S6a in the ESI.† All of the responses show favorable stability and consistency under the applied strain conditions. The strain dependence of the rise and recovery time is also obtained and plotted in Fig. S6b,† presenting no evident regularity. Maybe the response time of the devices is not accurately determined due to the limited time resolution of Keithley 4200, especially for the low current (<nA) measurement. However, how the strain would regulate carriers’ transport through the junction interface on the time scale and its underlying mechanism should also be very important and is worthy of further investigation.

Energy-band structures of the heterojunction are introduced to elucidate the modulation impact of the piezo-phototronic effect on the transport and photodetection properties in the devices. Fig. 4a shows the schematic band profile under strain-free and zero bias conditions. The electron affinity and bandgap of the 1D CdS NW are 3.87 eV and 2.43 eV, respectively, while the multi-layer WSe<sub>2</sub> flake has 4.06 eV electron affinity and 1.37 eV indirect bandgap.<sup>36,37</sup> Therefore, a conduction-band offset  $\Delta E_c = 0.19 \text{ eV}$  and a valence-band offset  $\Delta E_v = 0.86 \text{ eV}$  are presented at the heterojunction interface, which will influence the electrical transport behavior dramatically. Because of this band discontinuity, the barrier height for electrons diffusing from CdS to WSe<sub>2</sub> will be  $(qV_D - \Delta E_c)$ , while the barrier height for holes diffusing from WSe<sub>2</sub> to CdS is  $(qV_D + \Delta E_v)$ ;  $V_D$  is the overall built-in potential of the heterojunction. It can be observed that the barrier height for holes is much larger than that for electrons. Consequently, the output current of the device under forward bias mainly depends on the electron diffusion current. It is reported that the typical electron concentration of CdS nanowires is around  $10^{16}$ – $10^{17} \text{ cm}^{-3}$ , and the measured hole concentration in layered WSe<sub>2</sub> is about  $10^{11}$ – $10^{12} \text{ cm}^{-2}$  (corresponds to  $10^{18}$ – $10^{19} \text{ cm}^{-3}$ ).<sup>38–40</sup> Therefore it can be speculated that most of the built-in potentials fall in the CdS nanowire for the WSe<sub>2</sub>–CdS heterojunction. When a mechanical strain was introduced to the device, the piezoelectric polarization charges induced in CdS can redistribute the carriers at the vicinity of the heterojunction contact, thus affecting the local energy-band tilting at the interface.<sup>41,42</sup> Although the piezoelectric effect in atomically thin transition-metal dichalcogenides has also been successfully demonstrated, here the piezoresponse in WSe<sub>2</sub> could be ignored because of its larger thickness.<sup>43,44</sup> As shown in Fig. 4b, the energy band in both CdS and WSe<sub>2</sub> would bend downward under the influence of positive piezopolarization charges. As most of the built-in potentials fall in CdS and WSe<sub>2</sub> possesses a much higher carrier concentration, the magnitude of energy-band downward bending in WSe<sub>2</sub> could be negligible compared with that in CdS.<sup>45,46</sup> Therefore, a reduced overall barrier height  $qV_D$  could be obtained. Such realigned band tilting decreases the energy barrier for electron transport through the interface and the injection efficiency as

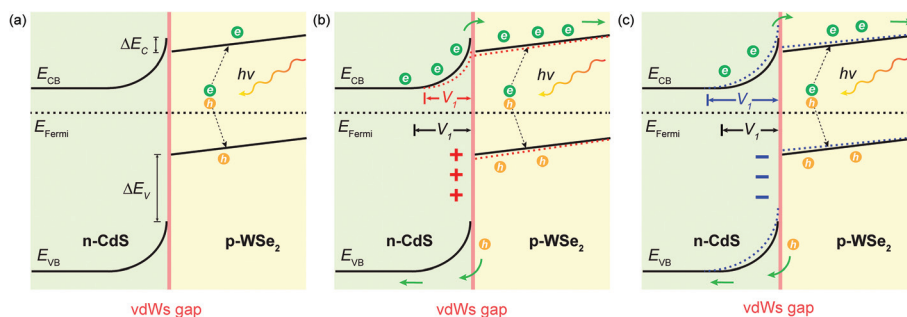


**Fig. 4** (a) Schematic band diagrams of WSe<sub>2</sub>–CdS under zero strain. The realigned energy-band profile at the interface with the presence of positive (b) and negative (c) piezoelectric polarization charges, which are denoted by red and blue dotted lines, respectively.

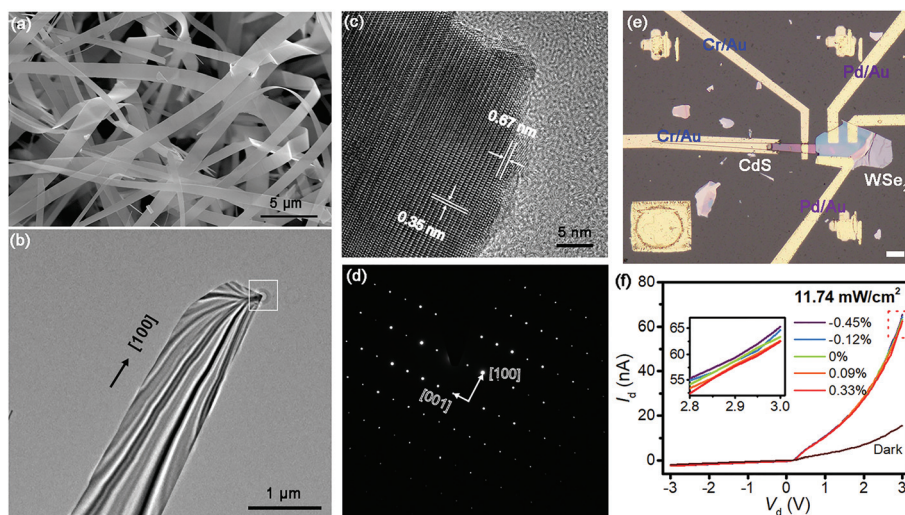


**Fig. 5** (a) The SEM image of as-grown CdS nanobelts. Low- (b) and high- (c) magnification TEM images of CdS nanobelts. (d) Selected area electron diffraction pattern of the white square area in (b). (e) Optical image of the fabricated WSe<sub>2</sub>-CdS nanobelt heterojunction; scale bar is 10  $\mu\text{m}$ . (f) Photoresponse in the device to 11.74  $\text{mW cm}^{-2}$  optical illumination under different strains; the inset shows the enlarged photocurrent in the red rectangle.

well as the overall collection of carriers are promoted, leading to an enhanced photocurrent. As the piezocharges can be generated at both ends of the CdS nanowire under mechanical strain, their influence on the CdS-Cr contact property should also be taken into account. In this case, negative piezocharges are created at the vicinity of the CdS-Cr interface, which will lead to an increased barrier height for electrons and a reduced photocurrent. This hypothesis is in contrast to the measured results in Fig. 3, which demonstrates that the piezo-phototronic modulation of the WSe<sub>2</sub>-CdS junction property should dominate the overall photodetection change. On the contrary, strain-induced negative piezopolarization charges at the WSe<sub>2</sub>-CdS interface will lead to the upward bending of the band in the CdS nanowire. In this case, the deformation of the band profile increases the barrier height for electrons and hinders the corresponding transport process, which deteriorates the photodetection performance as presented by the blue dotted line in Fig. 4c.

To further demonstrate the dominant role of the piezo-phototronic effect in the strain modulation of photodetection performance in the devices, a flexible WSe<sub>2</sub>-1D CdS nanobelt heterostructure on PET was fabricated. The nanobelts were prepared through the PVD method and the SEM image of the synthetic materials is shown in Fig. 5a. From the TEM characterization results in Fig. 5b-d, it is observed that CdS nanobelts possess good crystallinity and the growth direction is perpendicular to [0001]. Therefore the piezoelectric effect could be ignored when applying a uniaxial strain along the nanobelt length direction. The device fabrication of the WSe<sub>2</sub>-CdS nanobelt follows a similar procedure as that of the WSe<sub>2</sub>-CdS NW (Fig. S7†). Fig. 5e displays the OM image of the fabricated device on a flexible PET substrate. The photoresponse behavior of the device under 11.74  $\text{mW cm}^{-2}$  680 nm laser illumination and various mechanical strains is shown in Fig. 5f. The measured  $I_{\text{ds}}$  increases significantly upon illumination, but

the modulation impact of the strain on the detection performance is much weaker than that in WSe<sub>2</sub>-CdS NW devices. Here, the strain-induced change of the photocurrent mainly comes from the influence of the piezoresistive effect, contact resistance change or slight optical intensity variation when bending the flexible substrate.

## Conclusions

In summary, the piezo-phototronic effect in a flexible 2D WSe<sub>2</sub>-1D CdS mixed-dimensional vdWs heterostructure and its application in strain-modulated photodetection were studied. Tunability of the vdWs interface *via* mechanical strain was achieved, the photocurrent under 16.9  $\mu\text{W cm}^{-2}$  illumination was increased by  $\sim 110\%$  and the optimized photoresponsivity reaches up to 33.4  $\text{A W}^{-1}$  through applying a  $-0.73\%$  compressive strain. This enhancement originates from the realignment of local interface band tilting by strain-induced piezopolarization charges, which promotes the effective transport and overall collection of photoexcited carriers. This new coupling mode among semiconducting, piezoelectric and optoelectronic properties offers a new way to realize strain-tunable vdWs junctions other than with the conventional electrostatic gating. It is expected that the approach in this study might be extended to other artificial vdWs structures or superlattices, which may implement the high-performance 2D optoelectronics and enable the development of novel flexible devices.

## Experimental section

### Growth of CdS nanowires

CdS powder (Alfa Aesar 99.999%) was used as a precursor for the PVD synthesis of CdS nanowires in a three-temperature-

zone furnace. A quartz boat containing 150 mg of CdS was positioned in the center of the furnace tube (zone II), and silicon wafer deposited with 10 nm gold was located downstream (zone III) as the collecting substrate. The temperature in zone II was set at 850 °C and argon of 50 sccm was used as the carrier gas. The temperature in zone III was set at 650 °C and the whole synthesis process was maintained for 45 min.

### WSe<sub>2</sub>-CdS heterostructure assembly

The fabrication of the mixed-dimensional 2D WSe<sub>2</sub>-1D CdS NW vdWs heterostructure starts with the transfer of the CdS NW onto a PET substrate with an accurate transfer platform (Metatest, E1-T). Firstly, a dry transfer stamp (PPC film on PDMS on glass) was prepared. Then, the stamp was precisely lined up with the target CdS NW on a silicon substrate and annealed at 60 °C until the NW stuck securely on the stamp. Afterwards, the stamp was lifted up and lined up with the target position on PET and annealed at 130 °C for 5 min until the material (CdS NW on PPC) was securely deposited onto the substrate. Finally, the substrate was washed with acetone and isopropanol to remove PPC, and blown dry gently with N<sub>2</sub>. It is worth noting that the nanowire was intentionally placed in parallel to the length direction of PET to ensure that a uniaxial strain was induced when bending the substrate. The mechanically exfoliated WSe<sub>2</sub> nanosheet was precisely positioned onto the aforesaid CdS NW following the same procedure. All of the processes were performed under a microscope by using micro-manipulators to guarantee the transfer accuracy. Electrical contacts were patterned with electron beam lithography followed by electron beam deposition of Cr/Au (15 nm/50 nm) as the ohmic electrode for CdS, and the Pd/Au (15 nm/50 nm) layer for WSe<sub>2</sub>.

### Performance assessment and piezo-phototronic process test

All of the electrical tests were performed at room temperature using Keithley 4200-SCS in a shielded probe station. The 680 nm laser with tunable power was adopted as the optical source for heterojunction photosensing characterization, and the illumination intensity was calibrated with Thorlabs PM 100D. A home-made setup was prepared to study the piezo-phototronic process in the devices, by measuring the photo-response under specific mechanical strain and optical illumination power. The applied tensile and compressive strain could be introduced through bending PET upward and downward, respectively, with the magnitude proportional to the bending curvature and being controlled through the manipulation of the bending separation.

## Conflicts of interest

There are no conflicts to declare.

## Acknowledgements

This research was supported by the “Thousands Talents” program for pioneer researcher and his innovation team,

China, the National Natural Science Foundation of China (Grant No. 51702017, 11704032, 51432005, 5151101243, and 51561145021), the National Key R & D Project from the Minister of Science and Technology (2016YFA0202703 and 2016YFA0202704), the Beijing Municipal Science & Technology Commission (Z171100000317001), and the China Postdoctoral Science Foundation (2017M610837).

## References

- 1 X. Duan, C. Wang, A. Pan, R. Yu and X. Duan, *Chem. Soc. Rev.*, 2015, **44**, 8859–8876.
- 2 W. Choi, N. Choudhary, G. H. Han, J. Park, D. Akinwande and Y. H. Lee, *Mater. Today*, 2017, **20**, 116–130.
- 3 Q. H. Wang, K. Kalantar-Zadeh, A. Kis, J. N. Coleman and M. S. Strano, *Nat. Nanotechnol.*, 2012, **7**, 699.
- 4 D. Jariwala, V. K. Sangwan, L. J. Lauhon, T. J. Marks and M. C. Hersam, *ACS Nano*, 2014, **8**, 1102–1120.
- 5 J. M. Gonzalez and I. I. Oleynik, *Phys. Rev. B: Condens. Matter Mater. Phys.*, 2016, **94**, 125443.
- 6 K. S. Novoselov, A. Mishchenko, A. Carvalho and A. H. Castro Neto, *Science*, 2016, **353**, aac9439.
- 7 W. J. Yu, Y. Liu, H. Zhou, A. Yin, Z. Li, Y. Huang and X. Duan, *Nat. Nanotechnol.*, 2013, **8**, 952.
- 8 S. Bertolazzi, J. Brivio and A. Kis, *ACS Nano*, 2011, **5**, 9703–9709.
- 9 D. Jariwala, T. J. Marks and M. C. Hersam, *Nat. Mater.*, 2016, **16**, 170.
- 10 D. Kufer, I. Nikitskiy, T. Lasanta, G. Navickaite, F. H. L. Koppens and G. Konstantatos, *Adv. Mater.*, 2015, **27**, 176–180.
- 11 G. Konstantatos, M. Badioli, L. Gaudreau, J. Osmond, M. Bernechea, F. P. G. de Arquer, F. Gatti and F. H. L. Koppens, *Nat. Nanotechnol.*, 2012, **7**, 363.
- 12 D. Jariwala, V. K. Sangwan, C.-C. Wu, P. L. Prabhuramirashi, M. L. Geier, T. J. Marks, L. J. Lauhon and M. C. Hersam, *Proc. Natl. Acad. Sci. U. S. A.*, 2013, **110**, 18076–18080.
- 13 M.-L. Tsai, S.-H. Su, J.-K. Chang, D.-S. Tsai, C.-H. Chen, C.-I. Wu, L.-J. Li, L.-J. Chen and J.-H. He, *ACS Nano*, 2014, **8**, 8317–8322.
- 14 Y. Lin, X. Li, D. Xie, T. Feng, Y. Chen, R. Song, H. Tian, T. Ren, M. Zhong, K. Wang and H. Zhu, *Energy Environ. Sci.*, 2013, **6**, 108–115.
- 15 X. Li, W. Chen, S. Zhang, Z. Wu, P. Wang, Z. Xu, H. Chen, W. Yin, H. Zhong and S. Lin, *Nano Energy*, 2015, **16**, 310–319.
- 16 Y. Wan, J. Xiao, J. Li, X. Fang, K. Zhang, L. Fu, P. Li, Z. Song, H. Zhang, Y. Wang, M. Zhao, J. Lu, N. Tang, G. Ran, X. Zhang, Y. Ye and L. Dai, *Adv. Mater.*, 2018, **30**, 1703888.
- 17 D. Jariwala, S. L. Howell, K.-S. Chen, J. Kang, V. K. Sangwan, S. A. Filippone, R. Turrissi, T. J. Marks, L. J. Lauhon and M. C. Hersam, *Nano Lett.*, 2016, **16**, 497–503.

- 18 H. Yang, J. Heo, S. Park, H. J. Song, D. H. Seo, K.-E. Byun, P. Kim, I. Yoo, H.-J. Chung and K. Kim, *Science*, 2012, **336**, 1140–1143.
- 19 P. Lin, X. Yan, F. Li, J. Du, J. Meng and Y. Zhang, *Adv. Mater. Interfaces*, 2017, **4**, 1600842.
- 20 Y. Zhang, X. Yan, Y. Yang, Y. Huang, Q. Liao and J. Qi, *Adv. Mater.*, 2012, **24**, 4647–4655.
- 21 Y.-F. Lin, J. Song, Y. Ding, S.-Y. Lu and Z. L. Wang, *Appl. Phys. Lett.*, 2008, **92**, 022105.
- 22 Z. Liu, M. Amani, S. Najmaei, Q. Xu, X. L. Zou, W. Zhou, T. Yu, C. Y. Qiu, A. G. Birdwell, F. J. Crowne, R. Vajtai, B. I. Yakobson, Z. H. Xia, M. Dubey, P. M. Ajayan and J. Lou, *Nat. Commun.*, 2014, **5**, 5246.
- 23 A. Castellanos-Gomez, M. Buscema, R. Molenaar, V. Singh, L. Janssen, H. S. J. van der Zant and G. A. Steele, *2D Mater.*, 2014, **1**, 011002.
- 24 L. Wang, I. Meric, P. Y. Huang, Q. Gao, Y. Gao, H. Tran, T. Taniguchi, K. Watanabe, L. M. Campos, D. A. Muller, J. Guo, P. Kim, J. Hone, K. L. Shepard and C. R. Dean, *Science*, 2013, **342**, 614–617.
- 25 P. Tonndorf, R. Schmidt, P. Böttger, X. Zhang, J. Börner, A. Liebig, M. Albrecht, C. Kloc, O. Gordan, D. R. T. Zahn, S. Michaelis de Vasconcellos and R. Bratschitsch, *Opt. Express*, 2013, **21**, 4908–4916.
- 26 C. Pan, S. Niu, Y. Ding, L. Dong, R. Yu, Y. Liu, G. Zhu and Z. L. Wang, *Nano Lett.*, 2012, **12**, 3302–3307.
- 27 O. Lopez-Sanchez, D. Lembke, M. Kayci, A. Radenovic and A. Kis, *Nat. Nanotechnol.*, 2013, **8**, 497.
- 28 P. Lin, X. Yan, Z. Zhang, Y. Shen, Y. Zhao, Z. Bai and Y. Zhang, *ACS Appl. Mater. Interfaces*, 2013, **5**, 3671–3676.
- 29 R. Zhu and R. S. Yang, *Nanotechnology*, 2014, **25**, 345702.
- 30 X. Wen, W. Wu, C. Pan, Y. Hu, Q. Yang and Z. Lin Wang, *Nano Energy*, 2015, **14**, 276–295.
- 31 Z. L. Wang, *Adv. Mater.*, 2012, **24**, 4632–4646.
- 32 W. Liu, A. Zhang, Y. Zhang and Z. L. Wang, *Nano Energy*, 2015, **14**, 355–363.
- 33 Y. Liu, Y. Zhang, Q. Yang, S. Niu and Z. L. Wang, *Nano Energy*, 2015, **14**, 257–275.
- 34 W. Z. Wu and Z. L. Wang, *Nat. Rev. Mater.*, 2016, **1**, 16031.
- 35 G. H. Ahn, M. Amani, H. Rasool, D. H. Lien, J. P. Mastandrea, J. W. Ager, M. Dubey, D. C. Chrzan, A. M. Minor and A. Javey, *Nat. Commun.*, 2017, **8**, 608.
- 36 J. Li and N. Wu, *Catal. Sci. Technol.*, 2015, **5**, 1360–1384.
- 37 K. Kim, S. Larentis, B. Fallahazad, K. Lee, J. Xue, D. C. Dillen, C. M. Corbet and E. Tutuc, *ACS Nano*, 2015, **9**, 4527–4532.
- 38 T. Zhai, X. Fang, L. Li, Y. Bando and D. Golberg, *Nanoscale*, 2010, **2**, 168–187.
- 39 H. Fang, S. Chuang, T. C. Chang, K. Takei, T. Takahashi and A. Javey, *Nano Lett.*, 2012, **12**, 3788–3792.
- 40 A. Allain and A. Kis, *ACS Nano*, 2014, **8**, 7180–7185.
- 41 C. Liu, M. Peng, A. Yu, J. Liu, M. Song, Y. Zhang and J. Zhai, *Nano Energy*, 2016, **26**, 417–424.
- 42 Y. Zhang, J. Zhai and Z. L. Wang, *Small*, 2017, **13**, 1702377.
- 43 W. Wu, L. Wang, Y. Li, F. Zhang, L. Lin, S. Niu, D. Chenet, X. Zhang, Y. Hao, T. F. Heinz, J. Hone and Z. L. Wang, *Nature*, 2014, **514**, 470.
- 44 W. Wu, L. Wang, R. Yu, Y. Liu, S. H. Wei, J. Hone and Z. L. Wang, *Adv. Mater.*, 2016, **28**, 8463–8468.
- 45 P. Lin, X. Chen, X. Yan, Z. Zhang, H. Yuan, P. Li, Y. Zhao and Y. Zhang, *Nano Res.*, 2014, **7**, 860–868.
- 46 P. Lin, Y. Gu, X. Yan, S. Lu, Z. Zhang and Y. Zhang, *Nano Res.*, 2016, **9**, 1091–1100.